Comparative Resonance Raman Study of Cytochrome *c* Oxidase from Beef Heart and *Paracoccus denitrificans*†

George E. Heibel,‡ Peter Hildebrandt,*,‡ Bernd Ludwig,§ Peter Steinrücke,∥ Tewfik Soulimane,⊥ and Gerhard Buse⊥

Max-Planck-Institut für Strahlenchemie, Stiftstrasse 34–36, D-45470 Mülheim a.d. Ruhr, Federal Republic of Germany, Institut für Biochemie, Abteilung Molekulare Genetik, J. W. Goethe-Universität, Robert-Mayer-Strasse 7–9, D-60335 Frankfurt 11, Federal Republic of Germany, Institut für Molekulare Biotechnologie, Beutenbergstrasse 11, D-07745 Jena, Federal Republic of Germany, and Institut für Biochemie, Rheinisch-Westfälische Technische Hochschule Aachen Klinikum, Pauwelsstrasse 30, D-52074 Aachen, Federal Republic of Germany

Received January 14, 1993; Revised Manuscript Received June 22, 1993®

ABSTRACT: Well-resolved, Soret band excited resonance Raman spectra were measured from the fully oxidized and fully reduced cytochrome *c* oxidase from beef heart and *Paracoccus denitrificans*. The vibrational patterns in the marker band region (1450–1700 cm^{-1}) were analyzed, and a complete assignment of heme *a* and heme a_3 vibrational modes is presented, permitting a detailed structural comparison of the mammalian and bacterial enzymes. Similar frequencies of the porphyrin modes for the reduced heme *a* and the reduced and oxidized heme a_3 are found, indicating a close relationship of the ground-state conformations in all oxidase species studied. In oxidized heme *a*, however, significant frequency differences are observed and interpreted in terms of a ruffled porphyrin structure in the three- and two-subunit forms of the *Paracoccus* enzyme compared to the planar heme *a* of beef heart oxidase. The structural distortions, which also perturb the conformation of the formyl substituent and its electronic coupling with the porphyrin, reflect the specific heme–protein interactions at heme *a*. Since in the fully reduced state heme *a* appears to be largely planar in all oxidase species, the redox-linked conformational transition requires a more drastic rearrangement of the heme *a*–protein interactions in the bacterial than in the mammalian oxidase. For both heme *a* and heme a_3 in the reduced state and for heme a_3 in the oxidized state, frequency, intensity, and bandwidth differences of the formyl stretching vibration and intensity differences of some porphyrin modes are noted between the three oxidase forms. The same modes are also affected by quaternary structure changes in the bovine oxidase caused by different detergents and isolation procedures. These effects are attributed to differences of the dielectric properties of the heme environment, due to subtle structural changes in the heme pockets, induced by protein–protein interactions of subunit III with subunits I and/or II.

Mammalian cytochrome *c* oxidase is a multiple redox center protein complex, normally isolated as a 13-subunit enzyme, residing in the inner mitochondrial membrane. It is responsible for the stepwise reduction of molecular oxygen via the oxidation of cytochrome *c*. This redox process is linked to an active transport of protons across the inner mitochondrial membrane. The protein complex contains three reducible sites, heme *a*, Cu_A, and a dioxygen binding, binuclear center consisting of heme a_3 and Cu_B (Wikström et al., 1981; Brunori et al., 1987; Malmström, 1990). Hemes *a* and a_3 share the same molecular structure (shown in Figure 1) but differ in their spectroscopic properties. As yet, crystals useful for highly resolved X-ray structure analysis have not been grown.

Steady progress in the understanding of mammalian cytochrome oxidase has been made (Babcock & Wikström, 1992), most usually through the study of beef heart cytochrome *c* oxidase (BOX),[1] and researchers have also turned to the study of noneukaryotic versions of the enzyme complex largely due to the smaller number of subunits in bacterial oxidases. Cytochrome oxidase from the bacterium *Paracoccus denitrificans* can be isolated as a two-subunit enzyme (POX2) (Ludwig & Schatz, 1980) or a three-subunit enzyme (POX3)

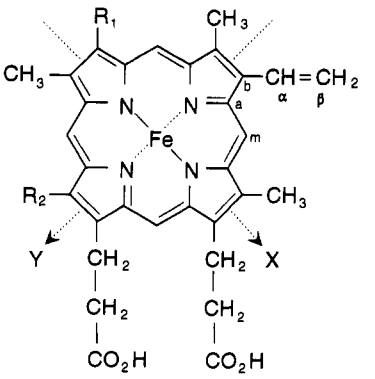

porphyrin *a* R_1 = -C(OH)$C_{16}H_{27}$, R_2 = -CH=O

PPIX R_1 = -CH=CH_2, R_2 = $-CH_3$

FIGURE 1: Molecular structures of protoporphyrin IX (PPIX) and porphyrin *a*. The pseudosymmetry axes are depicted. The axial ligands have been omitted for clarity.

† This work was supported in part by a grant from the state of Nordrhein-Westfalen (P.H.) and by the Deutsche Forschungsgemeinschaft (B.L.; LU 318/2-2).

* To whom correspondence should be addressed.
‡ Max-Planck-Institut für Strahlenchemie.
§ J. W. Goethe-Universität.
∥ Institut für Molekulare Biotechnologie.
⊥ Institut für Biochemie.

® Abstract published in *Advance ACS Abstracts*, September 1, 1993.

[1] Abbreviations: BOX, beef heart cytochrome *c* oxidase; POX2, POX3, two- and three-subunit cytochrome *c* oxidase from *Paracoccus dentrificans*; the subscripts "ox" and "red" denote the fully oxidized and fully reduced states, respectively; RR, resonance Raman; PPIX, iron protoporphyrin IX; 6cLS, six-coordinated low-spin; 6cHS, six-coordinated high-spin; 5cHS, five-coordinated high-spin.

0006-2960/93/0432-10866$04.00/0

(Haltia et al., 1988). Structural aspects of the *P. denitrificans* cytochrome oxidase have been reviewed recently (Ludwig, 1987; Saraste, 1990; Buse & Steffens, 1991). The originally purified POX2 has been found to be quite comparable to subunits I and II of BOX with respect to size, hydrophobicity, immunological cross reactivity, nucleotide sequence derived primary structure, and functional activity of inhibitors (Ludwig, 1987). This structurally simpler version of the mammalian enzyme has been shown to have oxygen reduction kinetics similar to those of BOX (Ludwig & Gibson, 1981). The physiological reductant for BOX is a soluble cytochrome *c*, whereas that for POX is believed to be a membrane-bound cytochrome c_{552} (Berry & Trumpower, 1985).

Investigations have been initiated to uncover the major differences of the two versions of the *Paracoccus* oxidase, differences which may give clues as to the function of the additional subunits in BOX. Studies which compared POX2 and POX3 found virtually identical energy transduction capabilities (Hendler et al., 1991), in analogy to similar findings of the nonessentiality of subunit III of BOX for the control of enzymatic activity (Gregory & Ferguson-Miller, 1988). The implication is that the third subunit of the bacterial enzyme may provide some of the regulatory functions of the oxidase, as have been postulated for apparently nonessential subunits of the mammalian oxidase (Hüther & Kadenbach, 1988). Indeed, a recent study (Pardhasaradhi et al., 1991) revealed differences in the respiratory control index between BOX and POX3, although the overall functional similarities between BOX and POX2 or POX3 suggest that the conformations of the active sites are quite similar. However, a detailed structural comparison of these enzymes on a molecular level is of particular importance since it may provide valuable information about the significance of the excess subunits in the mammalian enzyme for stabilizing specific active sites structures. Hence, appropriate methods are required which are capable of detecting even subtle structural differences of the redox centers in these enzymes.

Resonance Raman (RR) spectroscopy meets such requirements as it selectively probes the vibrational spectra of the heme groups. The high potential of this technique has been demonstrated by a large number of studies on heme proteins (Spiro & Li, 1988) as well as BOX itself (Babcock, 1988). We employ this technique for a detailed comparative analysis of BOX versus POX2 and POX3. In this paper we report our results on the fully oxidized and fully reduced forms of these enzymes, focusing on two spectral regions which provide complementary information about the conformation of the hemes and their interactions with the immediate protein environment. On the basis of high-quality spectra, we are able to resolve the strongly overlapping bands of the hemes *a* and a_3 and detect distinct spectral differences between the three forms of cytochrome *c* oxidase. The structural and functional implications of these findings are discussed.

MATERIALS AND METHODS

Sample Preparation. BOX was prepared by the method of Soulimane and Buse (unpublished results). Bovine heart mitochondria were prepared according to Crane et al. (1956) with several modifications. The sedimented mitochondria were homogenized in TS buffer (0.05 M Tris-HCl, 0.66 M sucrose, pH 7.6) and diluted to a protein concentration of 30 mg/mL. BOX, solubilized in 0.1% Triton X-100 or 0.05% dodecyl maltoside, buffered to pH 7.6, 10 mM Tris-HCl, was isolated by fractionated solubilization with subsequent chromatography on an anion exchanger (Q-Sepharose, Pharmacia). The phospholipid content was 44.8 ± 3.4 phosphorus atoms per dimer. BOX, solubilized in 1% cholate, buffered to pH 7.6 with 0.1 M phosphate, was isolated by fractionated solubilization with DOC (sodium desoxycholate) followed by repeated precipitation with $(NH_4)_2SO_4$. Triton X-100 and dodecyl maltoside solubilized enzyme showed monophasic/fast cyanide binding kinetics and high TN_{max} (600 s^{-1} in 0.05% dodecyl maltoside at 25 °C), demonstrating the homogeneity of the preparation. In contrast, the cholate solubilized enzyme showed multiphasic/slow cyanide binding kinetics and lower TN_{max} (120 s^{-1} in 0.05% cholate at 25 °C). Preparation and purity characterization of POX2 and POX3 were carried out according to Ludwig and Schatz (1980) and Haltia et al. (1988), respectively. These oxidases were diluted in 20 mM dodecyl maltoside, pH 7.6.

All preparations were shock frozen in liquid nitrogen and stored at −60 °C until immediately before spectral acquisition, at which time the sample was thawed and diluted with the appropriate buffer to an optical density of 1.0 at the excitation wavelength. Unless otherwise stated, the Triton X-100 preparation was used for the RR experiments.

Spectral Acquisition. Laser excitation at 413.1 and 406.7 nm was provided by a Kr^+ ion laser (Spectra Physics). Laser power at the sample was 25–30 mW. Scattered light was collected at 90° from a rotating quartz cuvette. The scattered light was focused onto the entrance slit of a Spex 1404 double monochromator with a spectral resolution of 3 cm^{-1}. The spectra were recorded upon repetitive scanning with a step size of 0.2 cm^{-1} and an acquisition time of 1.0 s/point. A photon counting system equipped with a cooled photomultiplier tube (RC 31034/76) was used to collect the signal. The dual channel detection technique (Rosseau, 1981; Hildebrandt & Stockburger, 1989) was used for the purpose of comparing the two- and three-subunit bacterial oxidases. All spectra were recorded at room temperature. Minor time-dependent spectral changes were observed after 1–2 h in the RR experiment as discussed in the text. Thus, the samples were replaced approximately each hour. It was verified that the spectra obtained from different samples and batches were identical, demonstrating the reproducibility of the results.

Data Handling. Spectra displayed are the sum of 15–20 scans for POX2 and POX3, 30 scans for BOX with 413-nm excitation, and 10 scans for BOX_{ox} with 406-nm excitation and BOX_{ox} in cholate, each scan requiring 20 min. The fluorescence background was removed by polynomial subtraction. For the spectra shown in this paper (except BOX_{ox} in cholate and BOX_{ox} at 406-nm) we have employed a filter to lower the level of high-frequency noise. Subtraction of filtered spectra from the original spectra yielded evenly distributed noise with an amplitude of 0.5–1.0% of the average number of counts in the unfiltered spectra. Thus, this procedure did not add or remove any information from the spectra nor did it affect the results of the fitting procedure.

Band Fitting. Spectra were analyzed with an interactive band fitting program utilizing the Marquardt algorithm for least-squares convergence, using a Lorentzian line shape. Other line shapes (Gaussian or Voigt functions) gave significantly worse fits, as found for other heme proteins (Hildebrandt & Stockburger, 1989; Hildebrandt et al., 1992). Band parameters were obtained by progressively lowering the respective damping constants until the difference between the simulated and measured spectra was within the noise level of the measured spectrum. The resulting bands in the spectra displayed in Figures 5 and 6, for example, had standard deviations which averaged 0.5 cm^{-1} in frequency, 1.4 cm^{-1} in

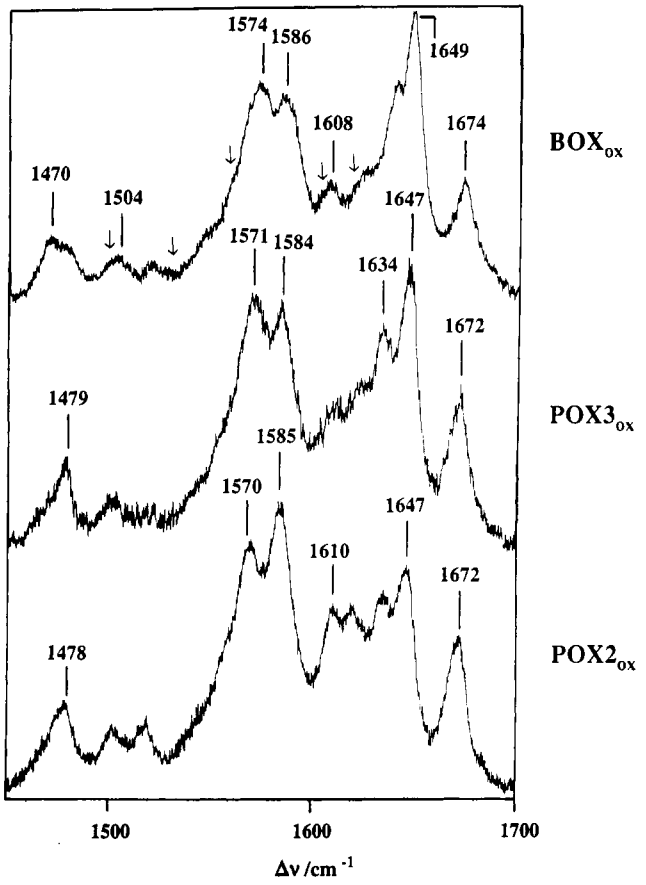

FIGURE 2: Resonance Raman spectra of (A) BOX_{ox}, (B) $POX3_{ox}$, and (C) $POX2_{ox}$ in the spectral region from 1450 to 1700 cm^{-1} obtained with 413-nm excitation. Peak positions are indicated by numbers and possible "hidden" components denoted with arrows.

band width, and 17% in intensity. In Figures 9 and 10, the standard deviations of band frequencies were better than 0.5 cm^{-1}, of bandwidths 1.0 cm^{-1}, and intensities 8%. For spectral regions containing many bands, specifically two spectral regions at ca. 1500 cm^{-1} of Figure 5 (ν_3 region) and ca. 1620 cm^{-1} of Figure 6 (vinyl stretching region) the fit quality was worse. However, for isolated bands, such as the 1649.0- and 1673.6-cm^{-1} bands (formyl stretching) in Figure 4, these parameters were better than 0.1 cm^{-1} in frequency, 0.2 cm^{-1} in band width, and 2% in intensity.

RESULTS AND DISCUSSION

Figure 2 displays the RR spectra in the high-frequency region of the fully oxidized states of cytochrome *c* oxidase from beef heart (BOX_{ox}) and *P. denitrificans* in the two- ($POX2_{ox}$) and three-subunit forms ($POX3_{ox}$) using the 413-nm excitation line. This spectral region is of particular interest since it includes bands which provide direct information about the geometry of the heme and the interactions of the heme substituents with adjacent amino acids of the heme pockets (Babcock, 1988). In the spectral region between 1450 and 1700 cm^{-1} (Figure 2), the three enzymes exhibit pronounced differences including intensity changes and frequency shifts. For example the broad peaks at 1568 and 1585 cm^{-1} shift down ~3 and ~1 cm^{-1} in the bacterial compared to the mammalian cytochrome *c* oxidase. On the other hand, the gross vibrational structure seems to be quite similar in BOX_{ox} and $POX3_{ox}$. In $POX2_{ox}$, however, the peak at ~1585 cm^{-1} is now the strongest in the RR spectrum and the bands between 1610 and 1630 cm^{-1} have strongly increased. The comparison with the RR spectrum of $POX2_{red}$ (Figures 9 and 10), excited at the same wavelength, clearly rules out that these differences are due to contributions from the reduced form. The RR spectrum of BOX_{ox} in this region is in good agreement with those reported earlier [Babcock & Salmeen, 1979; the "fast" form of BOX_{ox} reported by Schoonover et al. (1988)].

Vibrational Assignment of the Oxidized Species: High-Frequency Region. The frequencies of most of the (marker) bands in this region (Figure 2) are correlated with the core size of the porphyrin which in turn depends on the oxidation-, spin-, and ligation state of the heme iron (Spiro & Li, 1988). Among them are the A_{1g} modes ν_2 and ν_3, the B_{1g} modes ν_{10} and ν_{11}, and the B_{2g} mode ν_{28}, which are detectable in Soret-band excited spectra of heme proteins in general [mode numbering according to Abe et al. (1978)]. The low symmetry of type *a* hemes also induces RR activity into the E_u modes ν_{37} and ν_{38} which are forbidden in D_{4h} symmetry. Moreover, it is well established that the E_u modes can split, due to the nonequivalence of the *x* and *y* components of the electronic transition dipole moment which results from the *trans* disposition of the unsaturated vinyl and formyl substituents along the molecular *y* axis (Choi et al., 1983; Babcock, 1988; Willems & Bocian, 1984). In addition, the internal stretching vibrations of the formyl and vinyl substituents are resonance enhanced due to the conjugation of these substituents with the porphyrin π electron system.

The presence of both heme *a* and heme a_3 means that up to 22 bands can contribute to the spectral region displayed in Figure 2. In fact, a careful inspection of the RR spectra in Figure 2 reveals a complex vibrational structure. Most of the peaks are asymmetric and exhibit shoulders which indicate hidden band components (marked by arrows). However, application of a band fitting procedure does not yield unambiguous results in each part of the spectrum. Measurements of the parallel and perpendicular polarized RR spectra cannot provide additional information helpful for the analysis of the vibrational pattern, since in contrast to more symmetric porphyrins, the depolarization ratios of various symmetries obtained under Soret excitation conditions do not differ significantly in type *a* porphyrins (Choi et al., 1983; Babcock, 1988).

Hence, we have chosen a different approach by probing the RR spectrum with a second excitation wavelength (406 nm). This slight variation of the excitation condition results in small changes in resonance enhancement for the vibrational modes from the two different hemes and, within each heme, for modes with slightly different excitation profiles. Such spectra of BOX_{ox} are shown in Figures 3 and 4. It can be seen that some of the hidden band components are now more clearly identified. For example, the presence of two bands in the envelope at 1500 cm^{-1} is evident with comparison of the two spectra. The positions of the two bands in the 1475-cm^{-1} envelope and the bands on the low-frequency side of the 1575-cm^{-1} peak are better determined. The presence of two bands in the 1605-cm^{-1} peak and the 1620-cm^{-1} region is confirmed. The joint analysis of the 413- and 406-nm spectra allows for a more accurate determination of band components since the frequencies and the half-wdths must be the same in these two spectra. Thus, strict conditions could be imposed on the fitting procedure by using the same frequencies and bandwidths to simulate both the 413- and the 406-nm excited RR spectra. In this way, the effective standard deviations for the spectral parameters were significantly lowered. The results are shown in Figures 3 and 4.

Most of the bands can now be readily assigned following previous studies on cytochrome *c* oxidase and model compounds

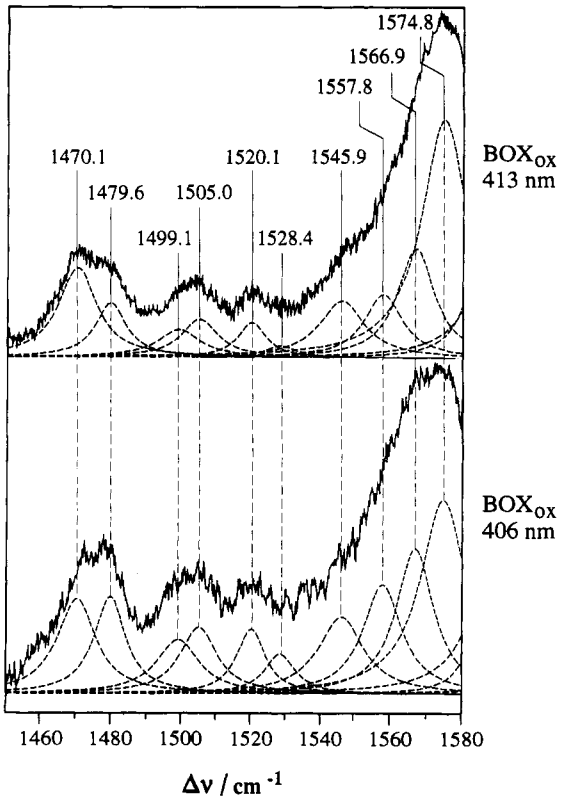

FIGURE 3: Resonance Raman spectra of BOX_{ox} in the spectral region from 1450 to 1580 cm^{-1} obtained with (**A**) 413-nm and (**B**) 406-nm excitation, together with the component Lorentz bands obtained by band fitting.

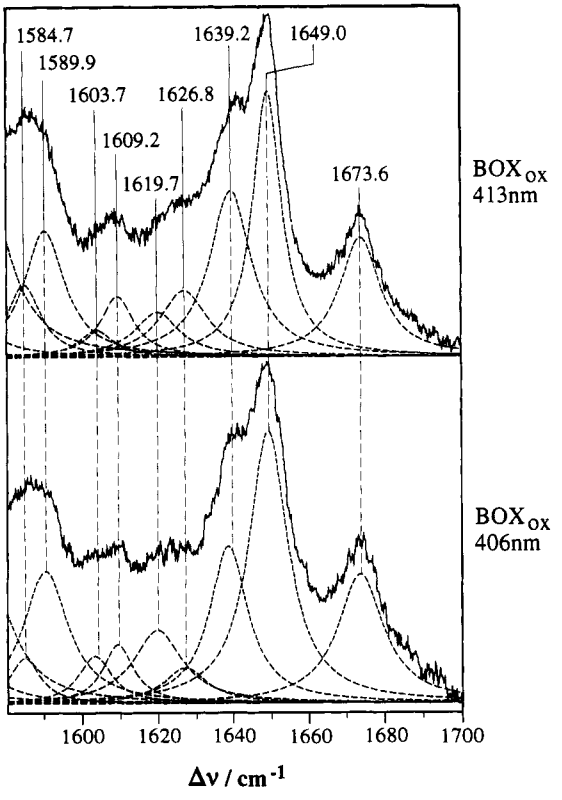

FIGURE 4: Resonance Raman spectra of BOX_{ox} in the spectral region from 1580 to 1700 cm^{-1} obtained with (**A**) 413-nm and (**B**) 406-nm excitation, together with the component Lorentz bands obtained by band fitting.

(Choi et al., 1983; Babcock, 1988). There is general agreement among these groups as to the positions and identities of the most easily observed bands (ν_2, ν_3, ν_{10}, ν_{11}, and ν_{28} for each

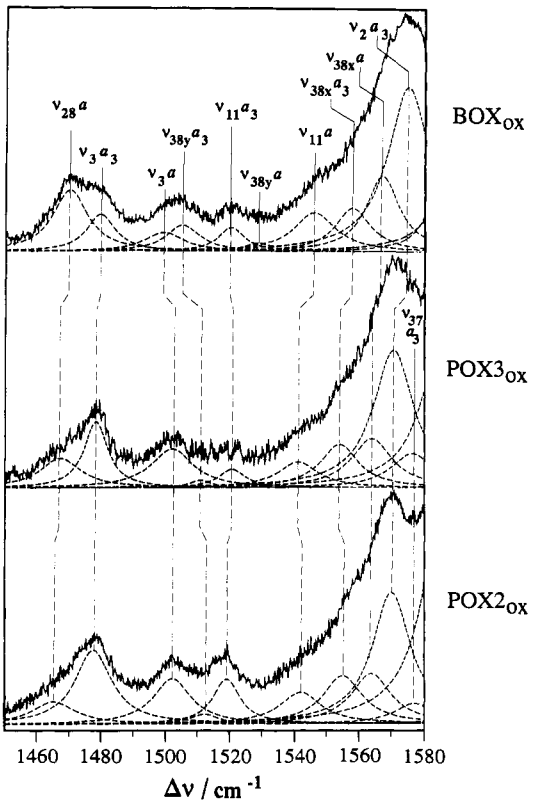

FIGURE 5: Resonance Raman spectra of (**A**) BOX_{ox}, (**B**) $POX3_{ox}$, and (**C**) $POX2_{ox}$ in the spectral region from 1450 to 1580 cm^{-1} obtained with 413-nm excitation, together with the component Lorentz bands obtained by band fitting.

heme). The classic trend of the heme a_3 marker band frequency downshifting with respect to heme *a* is seen, related to the larger porphyrin core size of the 6cHS heme a_3 compared to the 6cLS heme *a* (Parthasarathi et al., 1987; Babcock, 1988). Also the assignment of the formyl stretching vibrations is straightforward, and the 1649.0- and 1673.6-cm^{-1} bands are attributed to hemes *a* and a_3, respectively.

The E_u mode ν_{38} mode is expected split in type *a* porphyrins, whereas this has been observed for ν_{37} only in one reduced model compound [$(Im_2H)_2$Fe(II)porphyrin *a*; Choi et al., 1983)]. We assign the pair of bands at 1567 and 1558 cm^{-1} to the ν_{38x} mode of hemes *a* and a_3 respectively, and the pair at 1528 and 1507 cm^{-1} to the ν_{38y} mode of these hemes, respectively. If we assume a completely symmetric splitting of this mode, this results in a center frequency for ν_{38} of heme *a* at 1547 cm^{-1} and of heme a_3 at 1532 cm^{-1}. This is in agreement with the core size correlation which the center frequency is expected to obey.

The vinyl stretching vibration for each heme is expected to be observed at *ca.* 1620 cm^{-1}, as has been detected by several groups using Soret band excitation (Choi et al., 1983; de Paula et al., 1990). These bands appear in a crowded spectral region and were not resolved from each other in previous studies. However, a variation in excitation wavelength allows a more accurate determination of the positions of two bands in BOX_{ox} (Figure 4; *ca.* 1620 and 1627 cm^{-1}), which are assigned to the substituent vinyl stretching vibrations. In the next section we propose an assignment of the vinyl stretches to the individual hemes. The assignments are summarized in Table I.

Extension of the Assignment to P. denitricans Cytochrome Oxidases. The RR spectra of BOX_{ox}, $POX3_{ox}$, and $POX2_{ox}$ are shown in slightly expanded views in Figures 5 and 6. Included in these figures are the fitted Lorentz bands. The

Table I: High-Frequency Assignments for Oxidized Beef Heart and *Paracoccus* Oxidases[a]

	beef heart		*P. denitrificans* three subunits		*P. denitrificans* two subunits	
heme *a* mode	frequency	width	frequency	width	frequency	width
$\nu_{C=O}$ *a*	1649.0	9.2	1646.6	10.4	1647.5	9.2
					1643.4	8.3
ν_{10} *a*	1639.2	13.4	1634.1	12.1	1635.1	13.4
$\nu_{C=C}$ *a*	1626.8	15.1	1622.7	15.2	1623.6	14.7
ν_{37} *a*	1603.7	11.0	1603.1	13.1	1602.4	13.2
ν_2 *a*	1589.9	13.3	1585.4	15.0	1585.4	15.5
ν_{38_x} *a*	1566.9	12.6	1563.8	15.2	1563.7	14.6
ν_{11} *a*	1545.9	15.9	1541.1	15.2	1541.9	15.4
ν_{38_y} *a*	1528.4	10.8	not observed		not observed	
ν_3 *a*	1499.1	14.8	1501.9	15.7	1501.9	14.2
ν_{28} *a*	1470.1	13.1	1467.3	15.2	1465.2	16.4
heme a_3 mode	frequency	width	frequency	width	frequency	width
$\nu_{C=O}$ a_3	1673.6	13.2	1671.6	11.8	1671.4	11.3
$\nu_{C=C}$ a_3	1619.7	14.6	1621.5	14.8	1619.0	14.5
ν_{10} a_3	1609.2	10.8	1609.9	11.7	1609.4	9.5
ν_{37} a_3	1584.7	9.8	1576.2	15.1	1576.9	14.2
ν_2 a_3	1574.8	15.5	1570.4	15.1	1570.0	14.4
ν_{38_x} a_3	1557.8	13.4	1553.9	14.2	1554.9	14.7
ν_{11} a_3	1520.1	9.8	1520.6	9.9	1518.8	10.0
ν_{38_y} a_3	1505.0	12.8	1510.7	8.2	1511.9	10.7
ν_3 a_3	1479.6	10.8	1478.2	8.7	1477.5	13.6

[a] All numbers are given in cm^{-1}.

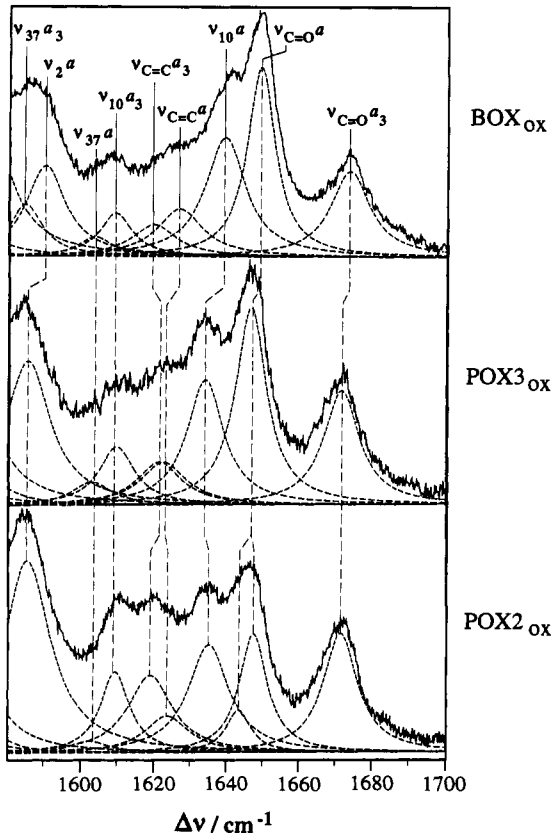

FIGURE 6: Resonance Raman spectra of (A) BOX_{ox}, (B) $POX3_{ox}$, and (C) $POX2_{ox}$ in the spectral region from 1580 to 1700 cm^{-1} obtained with 413-nm excitation, together with the component Lorentz bands obtained by band fitting.

band fitting yields similar standard deviations as in the case of BOX. The spectral parameters of $POX3_{ox}$ and $POX2_{ox}$ are listed in Table I. The assignments follow directly by comparison with the spectra of BOX_{ox}. We are unable to locate the very weak mode ν_{38_y} of heme *a* for either bacterial oxidase, although we note that this band does not appear to lie below 1530 cm^{-1}. It is more likely that this mode is buried in the low-frequency side of ν_{11} for heme *a*. Thus the splitting in ν_{38} for heme *a* of the bacterial oxidases appears to be reduced.

In the oxidized two-subunit enzyme, no satisfactory simulation of the spectrum in the region between 1645 and 1655 cm^{-1} was possible with only one component. Instead, the band fitting procedure reveals two bands at 1647 and 1643 cm^{-1}. We assign the lower frequency band to a heme *a* formyl stretch, downshifted 4 cm^{-1} from the main heme *a* formyl stretch. Heme photoreduction is not a possible cause for this band, since there is no band in the reduced spectrum of the two-subunit bacterial enzyme at this position (see Figure 10).

Vibrational Assignment of the Oxidized Species: Low-Frequency Region. In the low-frequency region (Figure 7), the spectral differences between the mammalian and the bacterial enzymes are much smaller. They include the peak at ~330 cm^{-1}, the apparent width of which varies considerably in the three enzymes, and the peaks between 400 and 420 cm^{-1} which are clearly less structured in the bacterial enzymes. We have carried out a band fitting procedure on the low-frequency spectrum of each oxidase with the results in Table II.

The low-frequency spectra of BOX_{ox} reported by Choi et al. (1983) and Schoonover et al. (1988) using 413-nm excitation are in good agreement with the spectrum presented in Figure 3; however, there are distinct differences from that presented by Babcock and Salmeen (1979) using 442-nm excitation. That spectrum is dominated by a peak at 345 cm^{-1} which corresponds to the small peak at ~347 cm^{-1} in present spectra. Most likely this results from the selective enhancement of heme *a* or heme a_3 modes at 442- and 413-nm excitation, respectively, due to the closer proximity of the Soret transitions with respect of the excitation lines (Choi et al., 1983; Babcock, 1988). Consequently, we assign the main peak at 332 cm^{-1} to ν_8 of heme a_3, while ν_8 for heme *a* is assigned to the weaker shoulder at 347 cm^{-1}, which corresponds to the dominant peak observed at 442-nm excitation (Babcock & Salmeen, 1979). Other bands of the 442-nm spectra cannot be observed with 413-nm excitation. This is not surprising since the ν_8 band, which should be the strongest band of heme

Table II: Low-Frequency Bands for Oxidized Beef Heart and *Paracoccus* Oxidases[a]

			P. dentrificans			
	beef heart		three subunits		two subunits	
mode	frequency	width	frequency	width	frequency	width
	not observed		288.0	8.2	284.0	7.1
	291.7	8.6	295.8	8.8	290.5	6.8
	322.8	13.8	not observed		316.4	13.7
$\nu_8\, a_3$	332.3	12.3	331.9	12.7	332.0	11.9
	339.3	15.0	336.4	15.1	339.7	14.2
$\nu_8\, a$	347.0	11.9	347.8	14.3	348.7	12.6
	369.4	13.3	368.4	15.4	368.8	13.8
	387.6	9.2	386.2	8.8	389.6	7.6
$\delta C_bC_\alpha C_\beta\, a_3$	402.5	15.6	401.2	14.3	404.1	16.0
	416.7	17.4	411.5	14.1	416.1	16.2
	435.0	15.4	435.7	7.8	436.1	13.7

[a] All numbers are given in cm^{-1}.

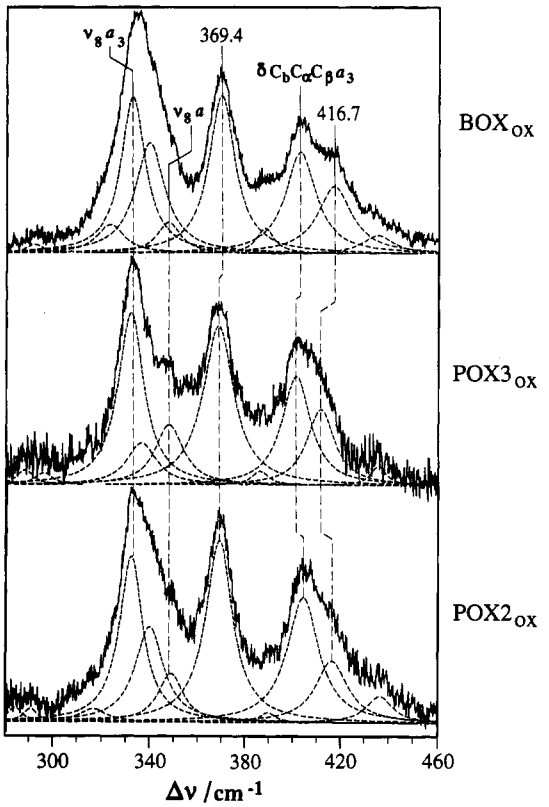

FIGURE 7: Resonance Raman spectra of (A) BOX_{ox}, (B) $POX3_{ox}$, and (C) $POX2_{ox}$ in the spectral region from 280 to 460 cm^{-1} obtained with 413-nm excitation, together with the component Lorentz bands obtained by band fitting.

a in this frequency range, is only detectable as a weak component by the band fitting analysis. Thus it is concluded that, except for this weak band, the low-frequency spectrum in Figure 7 exclusively displays the vibrational bands of heme a_3. The low-frequency RR spectrum of *Thermus thermophilus* cytochrome ba_3 reported by Einarsdóttir et al. (1989), recorded with 413-nm excitation, was also concluded to be comprised solely of heme a_3 and closely resembles the spectra in Figure 7.

The vibrational assignment of the low-frequency RR bands of BOX is not yet settled, although Choi et al. (1983) have provided assignments which account for the strongest bands in this region. The modes are believed to include significant contributions from bending vibrations of the peripheral substituents which in turn are involved in molecular interactions with adjacent amino acid residues. Thus, for many heme proteins this spectral range can be regarded as the characteristic fingerprint for the specific structure of the heme pocket (Hildebrandt, 1990). The vinyl bending vibrations of *b*-type hemes have been shown to contribute to two modes between 400 and 430 cm^{-1} (Uchida et al., 1988; Choi et al., 1982). In this region, we note two distinct bands at 416 and 402 cm^{-1} (BOX_{ox}) which show some of the most variable frequencies of any bands in the low-frequency range.

One of these bands (402 cm^{-1}) exhibits a trend with one of the high-frequency vinyl stretching bands, the component at ~1620 cm^{-1}, for each oxidase, such that the frequency of the 402-cm^{-1} band decreases as the frequency of the 1620-cm^{-1} vinyl stretching increases. This correlation is valid notwithstanding the somewhat lower accuracy of the fitting analysis in the vinyl stretching region of $POX3_{ox}$. This correlation can be rationalized by assuming that a higher stretching frequency corresponds to a more localized vinyl double bond which in turn may weaken the C_b–vinyl bending force constant, hence lowering the corresponding bending frequency. On the other hand, there is no comparable correlation with the higher frequency vinyl stretching band and the 416-cm^{-1} band. Thus we propose the assignment of the 402-cm^{-1} band to the vinyl bending and the 1619.7-cm^{-1} band to the vinyl stretching band to heme a_3 and, hence, the 1626.8-cm^{-1} band to heme *a* of BOX_{ox}. The vinyl stretching and bending modes of the bacterial oxidases are also assigned according to this correlation, leading to the assignments listed in Tables I and II.

Spectral Analysis of the Reduced Forms. Figure 8 displays the RR spectra of the fully reduced forms of the mammalian enzyme (BOX_{red}) and the bacterial enzymes ($POX2_{red}$ and $POX3_{red}$) in the region between 1450 and 1700 cm^{-1}, excited at 413 nm. The spectrum of BOX_{red} agrees well with that published previously at this excitation wavelength (Babcock et al., 1981). The spectral analysis encounters the difficulty that at 413-nm excitation both the (6cLS) heme *a* and (5cHS) a_3 contribute to the spectra to a comparable extent as reflected by the broad and asymmetric band envelopes. The careful visual inspection of the RR spectrum of BOX_{red} is already sufficient to identify several components with some confidence. A band fitting analysis of this spectrum alone does not allow a unique determination for all of the components. On the other hand, spectral resolution of the RR bands of heme *a* and heme a_3 is possible by comparing the 442-nm excited spectra of the mixed-valence, cyanide bound (Ching et al., 1985) or reduced, CO-bound forms (Argade et al., 1986) with the fully reduced form of BOX. The comparison of these spectra, obtained by the dual-channel Raman detection technique, demonstrates that each of the peaks at 1568, 1585, and 1611 cm^{-1} (Figure 8) must be composed of two band pairs at ~1565/1568, ~1579/1586, and ~1607/1611 cm^{-1}, respectively.

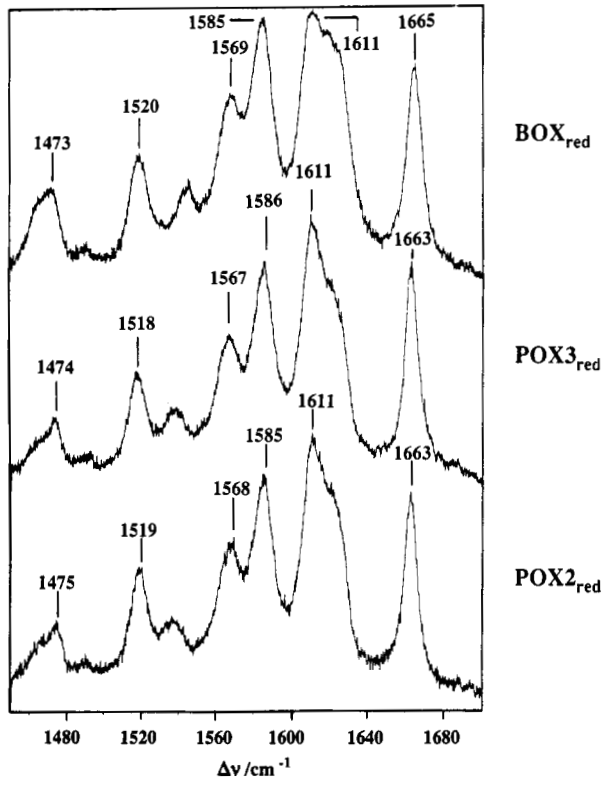

FIGURE 8: Resonance Raman spectra of (A) BOX_{red}, (B) $POX3_{red}$, and (C) $POX2_{red}$ in the spectral region from 1450 to 1700 cm^{-1} obtained with 413-nm excitation.

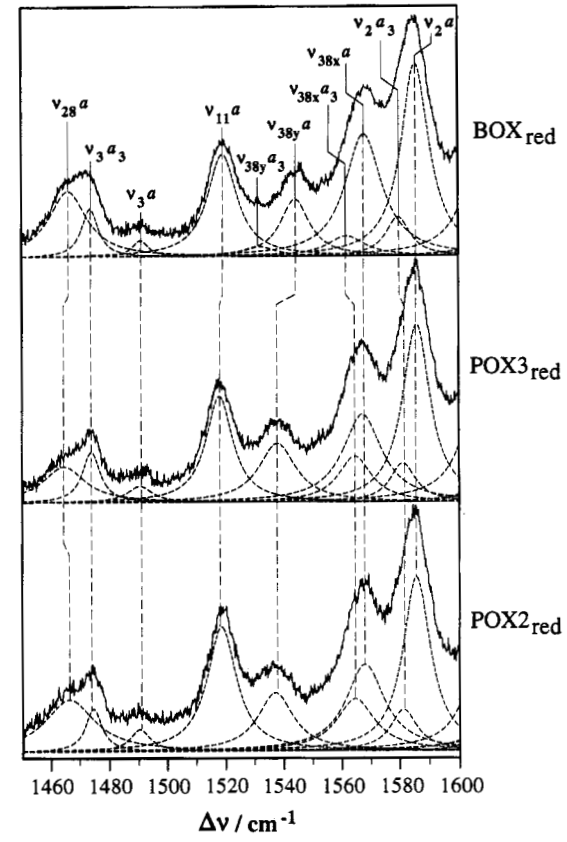

FIGURE 9: Resonance Raman spectra of (A) BOX_{red}, (B) $POX3_{red}$, and (C) $POX2_{red}$ in the spectral region from 1450 to 1600 cm^{-1} obtained with 413-nm excitation, together with the component Lorentz bands obtained by band fitting.

Combining this information with the band fitting analysis of the present RR spectra measured at 413-nm excitation provides a standard deviation of the band positions of better than 0.5 cm^{-1}, except for the more crowded region between 1620 and 1630 cm^{-1} where the standard deviation was 2.5 cm^{-1}.

The band fitting analysis of $POX3_{red}$ followed the same strategy as described for BOX_{red}, comparing the 442-nm spectra measured by Copeland et al. (unpublished data). For $POX2_{red}$, such data were not available, so that we used the spectral parameters obtained for $POX3_{red}$ as initial values for fitting the spectra of $POX2_{red}$. Small amounts of residual $POX2_{ox}$ and $POX3_{ox}$ (4–5%) in the reduced spectra were detected by the presence of the heme a^{3+} formyl stretching vibrations at 1647 cm^{-1} (Table I) and subtracted from Figures 9 and 10. The component Lorentz bands are shown in Figures 9 and 10 and their band parameters in Table IV. The heme *a* spectral parameters obtained for BOX_{red} in Table IV are in reasonable agreement with those of Sassaroli et al. (1989). We would also like to mention that the so obtained set of spectral parameters could be adopted to analyze the 442-nm excited RR spectra of the fully reduced and mixed-valence cyanide bound forms of BOX, recently measured by Copeland and co-workers (unpublished results).

Vibrational Assignments of the Reduced Enzymes. Most of the band assignments for the RR spectrum of BOX_{red} are generally agreed upon, on the basis of the body of data obtained from heme a_3 ligated species, variable wavelength studies, and model compound spectra (Centeno & Babcock, 1991; Choi et al., 1983; Argade et al., 1986; Ching et al., 1985; Willems & Bocian, 1984). Hence, in particular for most of the heme *a* modes (ν_{10}, ν_2, ν_{11}, ν_3, and ν_{28}) including the heme *a* formyl stretching vibration at 1609 cm^{-1}, we have adopted the assignments proposed previously. Also for heme a_3 the assignment of the modes ν_{10}, ν_2, and ν_3 as well as for the formyl stretching is widely accepted. The situation is less clear for the four bands between 1530 and 1570 cm^{-1} which must be attributed to split E_u modes of *a* (1567.8 and 1544.2 cm^{-1}) and a_3 (1561.8 and 1531.6 cm^{-1}). We assign these band pairs to the *x* and *y* components of ν_{38}, respectively. For the heme *a* band at 1568 cm^{-1}, Centeno and Babcock (1991) recently suggested an alternative assignment (ν_{37}) based on the RR spectrum excited in 605-nm absorption. This, however, would imply an unusually low frequency and strong resonance enhancement upon Soret band excitation for this mode. The ν_{38} bands at 1562 and 1532 cm^{-1} of heme a_3 have not been assigned previously. These bands are not intense, especially the latter mode, but the fit is unsatisfactory without the inclusion of these bands.

The vinyl stretching vibrations are at slightly different frequencies for the hemes *a* and a_3 whereas these bands are most often reported as being unresolved in both oxidation states of BOX (Babcock, 1988; Choi, 1983). In order to assign these bands to the vinyl groups of the individual hemes, we refer to the RR work by Ching et al. (1985), who presented essentially pure spectra of heme *a* and a_3. A careful inspection of these data suggests that in heme *a* the vinyl stretching appears at a higher frequency than in heme a_3, so that we assign the bands at 1625.8 and 1619.3 cm^{-1} to hemes *a* and a_3, respectively.

It is evident that the vibrational assignment as discussed for BOX_{red} can readily be extended to the bacterial oxidases. The only exception is the ν_{38y} mode of heme a_3 which may be hidden underneath the relatively broad 1537-cm^{-1} band in the spectra of $POX3_{red}$ and $POX2_{red}$, attributed to the ν_{38y} mode of heme *a*. This 1537-cm^{-1} band could not reliably be resolved into two components by the band fitting although the inclusion of a second band at aproximately 1528 cm^{-1} would

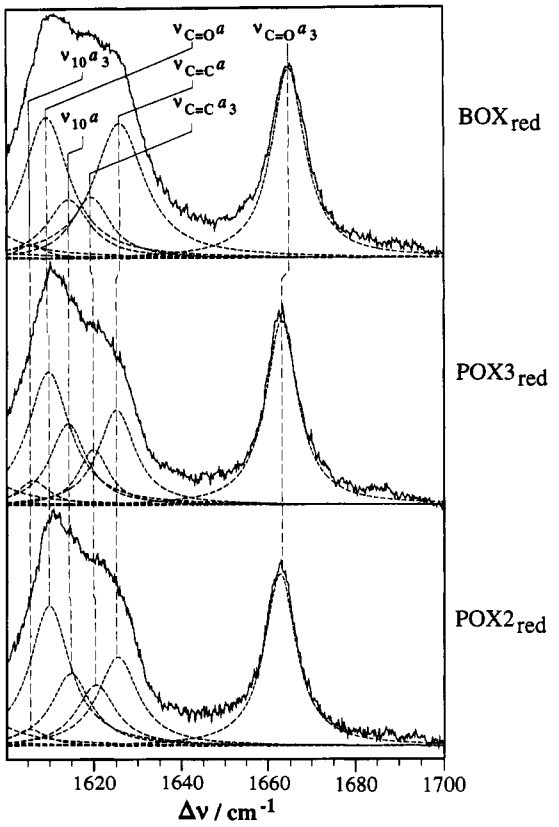

FIGURE 10: Resonance Raman spectra of (A) BOX_{red}, (B) $POX3_{red}$, and (C) $POX2_{red}$ in the spectral region from 1600 to 1700 cm^{-1} obtained with 413-nm excitation, together with the component Lorentz bands obtained by band fitting.

Table III: Deviations of Oxidized Marker Band Frequencies from Ideal Behavior[a]

mode	PPIX[b]	porphyrin a[b]	$BH_{ox}(a)$	$PD3_{ox}(a)$	$PD2_{ox}(a)$
		Heme a, Ferric, 6cLS			
ν_{10}	1640	0	−1	−6	−5
ν_{37}	1602	n.o.[c]	+2	+1	0
ν_2	1579	+9	+11	+6	+6
ν_{11}	1562	−9	−17	−21	−20
ν_{38}[d]	1554	−3	−7	−5	−6
$\Delta\nu_{38}$	n.o.[c]	22	39	<30	<30
ν_3	1502	+1	−3	0	0
ν_{28}	1469	+4	+1	−2	−4
		Heme a_3, Ferric, 6cHS			
mode	PPIX[e]	porphyrin a[e]	$BH_{ox}(a_3)$	$PD3_{ox}(a_3)$	$PD2_{ox}(a_3)$
ν_{10}	1610	−1	−1	0	−1
ν_{37}	1580	n.o.[c]	+5	−4	−4
ν_2	1559	+8	+16	+11	+11
ν_{11}	1545	−25	−25	−25	−26
ν_{38}[d]	1518	n.o.[c]	+14	+14	+14
$\Delta\nu_{38}$	n.o.[c]	n.o.[c]	52	43	43
ν_3	1480	−2	0	−2	−2

[a] All numbers are given in cm^{-1}. [b] Values are taken from Choi et al. (1983) for $Fe^{III}(ImH)_2PPIX$ and $Fe^{III}(ImH)_2Pa$. [c] Not observed. [d] The center frequency for those modes which display splitting was determined by assuming a symmetric splitting. [e] Values are taken from Choi et al. (1983) for $Fe^{III}(Me_2SO)_2PPIX$ and $Fe^{III}(Me_2SO)_2Pa$.

narrow the bandwidth of the neighboring ν_{38y} of heme a to give a value more in agreement with BOX_{red} (Table IV).

Spectral Differences between Mammalian and Bacterial Oxidases. The spectral differences between the three species include both band frequencies and widths as well as the RR intensities. Variations of the band intensities could conceivably be due to small alterations of the Soret transitions which in the bacterial enzymes are in fact red-shifted by 2 nm to 424

Table IV: High-Frequency Assignments for Reduced Beef Heart and *Paracoccus* oxidases[a]

heme a mode	beef heart		*P. dentrificans* three subunit		*P. dentrificans* two subunit	
	frequency	width	frequency	width	frequency	width
$\nu_{C=C}$ a	1625.8	14.0	1625.0	10.0	1625.2	11.0
ν_{10} a	1614.2	11.9	1614.0	9.9	1614.6	10.7
$\nu_{C=O}$ a	1609.2	12.6	1609.6	11.4	1609.7	11.1
ν_2 a	1585.5	11.6	1585.7	11.3	1585.6	11.4
ν_{38x} a	1567.8	15.3	1567.2	16.3	1567.9	16.2
ν_{38y} a	1544.2	12.1	1537.9	15.5	1537.1	14.8
ν_{11} a	1519.1	12.4	1517.9	11.2	1518.5	12.3
ν_3 a	1490.8	6.9	1490.5	10.3	1490.4	8.4
ν_{28} a	1466.1	16.0	1464.5	17.8	1466.4	20.5
heme a_3 model	frequency	width	frequency	width	frequency	width
$\nu_{C=O}$ a_3	1664.7	9.4	1662.9	8.8	1662.4	8.7
$\nu_{C=C}$ a_3	1619.3	10.8	1619.8	8.5	1620.3	10.7
ν_{10} a_3	1605.8	8.0	1606.1	8.9	1605.2	9.6
ν_2 a_3	1579.5	9.9	1581.1	10.6	1581.2	11.0
ν_{38x} a_3	1561.8	15.9	1564.6	14.1	1564.6	16.1
ν_{38y} a_3	1531.6	14.4	not obsd		not obsd	
ν_3 a_3	1473.6	6.9	1473.9	7.4	1474.5	6.7

[a] All numbers are given in cm^{-1}.

and 445 nm in the oxidized and reduced state, respectively. This shift may be responsible for the intensification of the A_{1g} modes ν_2 and ν_3 relative to the B_{1g} modes ν_{10} and ν_{11} in $POX3_{ox}$ and $POX2_{ox}$. For example, in heme a the ν_2/ν_{10} intensity ratio increases from 0.76 (BOX_{ox}) to 1.15 ($POX3_{ox}$) and 1.79 ($POX2_{ox}$). In the reduced form, the energy difference between the excitation line (413 nm) and the Soret transition is much larger so that a small shift of the latter is not expected to affect the resonance conditions significantly. In fact, the intensity differences between BOX_{red} and $POX3_{red}$ ($POX2_{red}$) are much smaller than in the oxidized state.

Prior to a discussion of the heme specific spectral differences, it is necessary to comment on some pecularities of the marker bands, generally noted for type a iron porphyrins in the oxidized state. As can be seen from Table III, in a simple protein-free, ferric 6cLS or 6cHS porphyrin a, the mode ν_2 is significantly higher and the mode ν_{11} drastically lower in frequency than in the corresponding PPIX complexes. Choi et al. (1983) interpreted the deviations for these two modes, which include high contributions from the C_bC_b (see Figure 1) stretching vibrations, to an alteration of the conjugation pathway within the porphyrin via the participation of the formyl and vinyl substituents. This is observed to have a qualitatively different effect on the stretching force constants of the B_{1g} modes (ν_{11}) and the A_{1g} mode (ν_2, ν), corresponding to the out-of-phase and in-phase stretching vibrations of the adjacent C_bC_b bonds (see Figure 1). Thus, the frequencies of these modes as well as the splitting of the ν_{38} mode should be a useful guide to gauge the extent of electronic coupling between the porphyrin and its substituents and, thus indirectly, the extent of protein–heme interactions.

The comparison with the data of ferric porphyrin a model compounds shows a relatively good agreement with the RR frequencies of BOX_{ox}. The deviations from the PPIX model for the frequency of the mode ν_{11} and the splitting of ν_{38} are larger in BOX_{ox}. This implies that interactions with the protein environment strengthen the electronic coupling of the conjugated substituents with the porphyrin macrocycle. Most likely, these interactions predominantly affect the formyl group since the downshift of ν_{11} in BOX_{ox} compared to the porphyrin a model complex is paralleled by a downshift of the formyl

stretching vibration (17 cm^{-1}; Choi et al., 1983). This may also reflect mixing of porphyrin skeleton vibrations and the formyl stretching as recently pointed out by Han et al. (1991). A comparison of the behavior of the marker bands of the reduced PPIX and porphyrin *a* model compounds (Choi et al., 1983) leads conclusions similar to those reached for the oxidized species, namely, that ν_2 increases, ν_{11} decreases strongly, and ν_{38} undergoes splitting when porphyrin *a* is compared to PPIX. In BOX_{red}, we note that these trends are partially reversed, indicating a decrease in the porphyrin/substituent electronic coupling in the protein. This remains true in spite of the strong hydrogen which is believed to be formed between the reduced heme *a* formyl group and an as yet unspecified donor (Babcock & Callahan, 1983).

Structural Differences in Heme a. The most pronounced spectral differences between the mammalian and the bacterial oxidases are observed in the oxidized state. These are, in particular, frequency shifts of the porphyrin skeleton modes by up to 5 cm^{-1}, implying that there are distinct differences in the ground state structure of heme *a*. Differences between between the oxidized mammalian and the bacterial enzymes have also been observed by EPR spectroscopy (Albracht et al., 1980; Aasa et al., 1976; Sievers et al., 1983). While for BOX_{ox} a g_z signal at 3.03 was observed, POX_{ox} exhibits a markedly lower value at 2.84. Such a lowering of the g_z value has been convincingly explained by a deprotonation or, more likely, a strong hydrogen bonding of one of the axial histidine ligands (Hosler et al., 1992). Hence, it is tempting to relate these findings to the changes in the RR spectra. A more basic axial ligand may increase the back-donation of electron density from the d_π orbitals of the iron to the e_g orbitals of the porphyrin, thereby affecting the frequencies of the vibrational modes. This has been experimentally verified in ferrous hemes (Partharasathi et al., 1987; Debois & Lutz, 1992). However, as demonstrated by Debois and Lutz (1992), the RR spectra of ferric PPIX compounds ligated by imidazole and deprotonated imidazoles are not affected in the marker band region indicating that back-donation is less efficient in the oxidized state. These data imply that a hydrogen-bonded or deprotonated histidine ligand is not the main origin for the observed frequency shifts in $POX3_{ox}$ and $POX2_{ox}$. The relative insensitivity of the RR spectrum toward the increased basicity of an axial ligand in the ferric hemes is line with the results obtained for cytochrome *c* oxidase from *Rhodobacter spheroids* (Hosler et al., 1992) or for cytochrome P-450 (ligation by a thiolate; Anzenbacher et al., 1989).

The bacterial enzymes reveal a decrease in the ν_{38} mode splitting and a frequency downshift of ν_2 which might indicate a weakening of electronic interactions with the conjugated substituents. However, the lowered ν_{11} frequency does not fit to this scheme. Moreover, the mode ν_{10} appears at much lower frequencies although it does not include a significant C_bC_b stretching contribution (Li et al., 1990). Apparently, there is another origin for these frequency shifts, associated with a structural perturbation of the porphyrin macrocycle.

An expansion of the heme *a* core size in the bacterial oxidases would cause a more or less uniform frequency downshift of all the marker bands, although the slight frequency upshift of ν_3 contradicts this interpretation. On the other hand, ruffling of the tetrapyrrole macrocycle has been shown to lower the marker band frequencies of the various modes to a different extent (Alden et al., 1989; Czernuszewicz et al., 1989; Shelnutt et al., 1991; Prendergast & Spiro, 1992). This heme distortion involves the alternate twisting of the pyrrole rings along the metal–nitrogen bond and has been observed in numerous heme protein crystal structures [references in Shelnutt et al. (1991)]. The most pronounced effect of heme ruffling in the RR spectra observed by these research groups is the downshift of the mode ν_{10}, while the downshifts of ν_2, ν_3, ν_{28}, and ν_{11} are clearly less. It is reasonable to assure that the tendencies which have been extensively studied in Ni-porphyrin are valid independent of the type of the metal, in analogy to the core-size relationships. Then one can easily rationalize, on a qualitative level, the observed frequency shifts in the $POX3_{ox}$ heme *a* skeletal modes (compared to BOX_{ox}) in terms of both a heme *a* ruffling and a weaker electronic coupling with the formyl and/or vinyl substituents. The marker band frequencies of the two-subunit bacterial enzyme are very similar to those of $POX3_{ox}$. This suggests that, as far as the heme *a* skeleton is concerned, the heme geometry is largely the same in $POX2_{ox}$ and $POX3_{ox}$, namely, ruffled.

The ruffling of the porphyrin and is accompanied by structural changes of the conjugated heme substituents. A frequency shift by 2.5 cm^{-1}, associated with an intensity reduction, is observed for the formyl stretching of $POX3_{ox}$ compared to BOX_{ox} pointing to altered (hydrogen-bonding) interactions of this substituent with the protein environment. In $POX2_{ox}$, even more drastic changes are noted for this mode which is split into two components at 1647 and 1643 cm^{-1}. Presumably, the lower frequency band represents a heme *a* population in which the formyl is in a more hydrogen-bonded environment. It is not possible to decide whether or not these conformers differ with respect to their marker band frequencies. While in $POX2_{ox}$ the heme *a* vinyl stretching band is found essentially at the same position as in BOX_{ox}, the corresponding mode of $POX3_{ox}$ is downshifted by about 5 cm^{-1} and coincides with the corresponding band of heme a_3 at 1622 cm^{-1}. This frequency shift may either be due to changes of the tilting angle or inductive effects caused by nearby charged amino acid side chains. For each oxidase the bandwidths are relatively broad when compared to other protoporphyrin containing heme proteins, which may reflect high conformational flexibility of the heme *a* vinyl groups.

In the reduced state, the frequencies of all the heme *a* marker bands of the mammalian and the two bacterial oxidases are at essentially the same positions (except for the ν_{38y} mode), indicating a very similar heme *a* geometry. This agreement rules out a deprotonated or strongly hydrogen-bonded histidine ligand which would exert a pronounced influence on the porphyrin modes (Partharasathi et al., 1987; Debois & Lutz, 1992). Also the formyl and vinyl substituents exhibit a similar structure as suggested by the comparison of the corresponding stretching modes. The only notable difference is an intensity increase and a band narrowing of the vinyl stretching in $POX3_{red}$ and $POX2_{red}$.

Structural Differences in Heme a_3. The marker bands of heme a_3 of BOX_{ox} can readily be interpreted in a similar way as those of heme *a*. Again, the deviations of the frequencies from the expected behavior, i.e., the upshift of ν_2 and the increase of the ν_{38} splitting imply an enhanced porphyrin/substituent electronic coupling compared to the corresponding heme a_3 model compound (Choi et al., 1983), apparently induced by the interaction with the surrounding protein environment (cf. Table III). Evidently, these interactions are different in the bacterial enzymes since the above mentioned deviations are less pronounced than in BOX_{ox}.

The most important difference compared to heme *a*, however, is that the mode ν_{10} remains at the same position in BOX_{ox}, $POX3_{ox}$ and $POX2_{ox}$. Thus, a ruffling of the porphyrin as in the case of heme *a* is not indicated. Hence, we conclude

that the heme a_3 geometry is largely the same in all three enzyme species, which is in line with the similar vibrational pattern in the low-frequency region. This conclusion can also be extended to the reduced forms.

In both the oxidized and the reduced states, the ground-state structure of the vinyl substituents of heme a_3 is apparently the same as indicated by the invariant stretching frequencies. On the other hand, a drastic intensity increase (with respect to ν_2) is noted in $POX2_{ox}$ (0.65) compared to BOX_{ox} (0.26) or $POX3_{ox}$ (0.32). These intensity changes may reflect alterations of the dielectric properties in the immediate environment of these substituent due to the displacement of polar and/or nonpolar amino acids in the heme pocket (Hildebrandt et al., 1988).

This interpretation may also hold for downshift and band narrowing of the formyl stretching in both the reduced and oxidized forms of POX3 and POX2 compared to BOX. Taking into account previous results on the solvent dependence of the C=O stretching in chlorins (Koyama et al., 1986), the lowered frequencies in the bacterial enzymes indicate a slightly higher dielectric constant of the formyl environment.

Redox-Linked Structural Changes. The comparison of the RR spectra of BOX_{ox} and BOX_{red} and those of model compounds suggest that both the protein-bound heme *a* and heme a_3 exhibit a similar porphyrin geometry as in solution. As far as the structure of porphyrin *a* in solution can be regarded as planar, this should also be true for the hemes incorporated in the protein matrix of BOX_{ox} and BOX_{red}. This conclusion can be extended to the reduced forms of the bacterial enzymes (POX3, POX2) for both heme *a* and heme a_3 and for heme a_3 of the oxidized species, while for the oxidized forms of POX3 and POX3 the present data indicate a ruffled heme *a* geometry. This implies that the main conformational changes in the bacterial enzymes upon reduction include a relaxation of the heme *a* structure. This structural transition may be caused by the displacement of amino acid residues in the heme pocket, which in the oxidized state impose steric constraints on the heme *a* group via strong nonbonding, electrostatic and/or hydrogen-bonding interactions. Such interactions apparently also affect the structure of the heme *a* formyl substituent of the oxidized state, most clearly visible by the formation of a second formyl conformation in $POX2_{ox}$. The frequencies of the two C=O stretching vibrations in this species as well as of the corresponding mode of $POX3_{ox}$ suggest stronger hydrogen-bonding interactions than in BOX_{ox} while in the reduced state the structure and environment of this substituent apparently the same for all three enzyme species, pointing to similar heme–protein interactions in the heme pocket. This conclusion can be extended to the axial histidine ligands. Following the idea that one of these ligands is strongly hydrogen-bonded (or deprotonated) in POX_{ox} (Hosler et al., 1992), it is concluded that such interactions with a nearby proton acceptor are largely removed in the reduced state. No significant redox-linked conformational changes can be inferred from the RR spectra for the heme a_3.

Factors Controlling the Active Site Structure. Now we may discuss those structural elements which are responsible for the differences in the active site conformations of the three oxidase species. The comparison between the two- and three-subunit enzymes of *Paracoccus* allows an assessment of the structural importance of subunit III in this oxidase. The ground-state conformations of both heme *a* and heme a_3 in the oxidized and the reduced forms are quite similar (except for the additional $POX2_{ox}$ heme *a* formyl environment), and the main spectral differences refer to the relative RR intensities

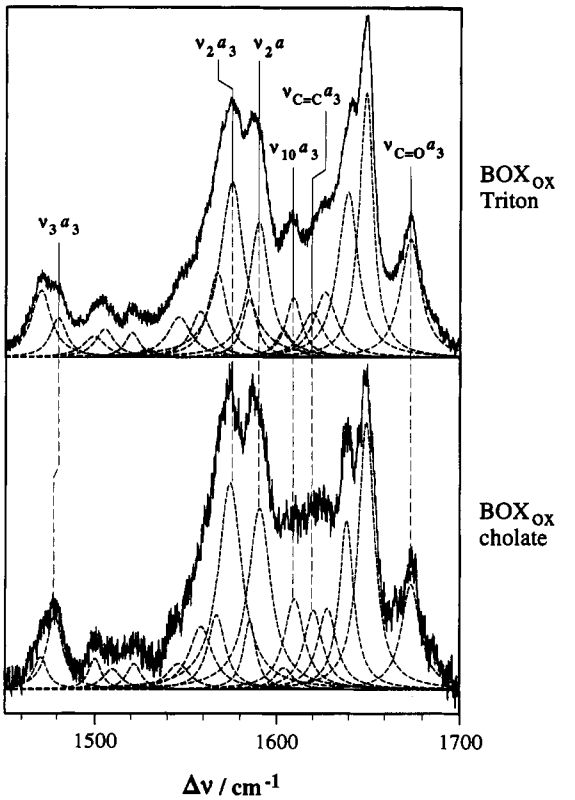

FIGURE 11: Resonance Raman spectrum of BOX_{ox} in (**A**) Triton X-100 and (**B**) cholate in the spectral region from 1450 to 1700 cm^{-1} obtained with 413-nm excitation.

but are clearly less pronounced than compared to the mammalian oxidase. Since the electronic transitions of POX3 and POX2 are identical, these differences are ascribed to environmental effects in the heme pocket. This implies that the protein–protein interactions at the interfaces between the subunit III and the subunits I and II are transduced to the active sites, ultimately leading to a modification of the effective dielectric constant, for example, via the displacement of amino acid residues or water molecules. It is interesting to note that qualitatively similar spectral changes which we ascribe to the effect of subunit III are also observed in BOX_{ox} using different detergent preparations.

Figure 11 compares the RR spectra of BOX_{ox} solubilized in Triton X-100 and in cholate. We note distinct changes of the relative intensities in the regions betwen 1470 and 1490 cm^{-1} (ν_3), 1560 and 1590 cm^{-1} (ν_2), and 1610 and 1630 cm^{-1} (vinyl stretching) while the frequencies are largely the same, implying identical ground-state conformations. It is unlikely that the different detergents interact directly with the hemes or their pocket environments. Rather, they may affect the protein–protein interactions between the various subunits. Such interactions may then result in subtle perturbations of the protein environment in the active sites, thereby influencing the relative intensities. This interpretation is in line with the conclusions drawn by Schoonover et al. (1988) from a comparative RR study on the "slow" and "fast" forms of BOX_{ox}.

It is now interesting to note that most of the detergent-dependent spectral changes occur in those bands which also reveal differences comparing $POX2_{ox}$ and $POX3_{ox}$, such as the vinyl stretching, ν_{10}, and ν_3 of heme a_3. This suggests that the crucial subunit interfaces which mediate the detergent-induced changes of the quaternary structure to the heme pockets are those between the subunits I and III and/or II and III. In this context we would like to add that slow changes

on the level of the quaternary structure may be the origin for the small time-dependent spectral changes observed during the RR experiments which primarily involve intensity changes in the vinyl stretching region.

While the spectral differences between POX2 and POX3 can readily be attributed to the effect of subunit III, the significant differences in the ground-state conformations of the oxidized forms of BOX and POX3 may either be due to the remaining subunits in BOX, implying a much more pronounced effect on the active site structure than for subunit III, or to the differences of subunit III between the mammalian and bacterial oxidases. The differences may also be found within subunit I itself, which contains the two heme groups as well as Cu_B and is highly conserved among species examined, except for an extra loop between helices I and II, consisting of 17 amino acids, found only in *P. denitrificans* (Saraste, 1990). Whether or not this loop is related to the structural differences in the active site remains to be investigated.

Recently, progress has been made in identifying those histidines which coordinate the metal centers by using point mutants of cytochrome *c* oxidase from *R. sphaeroides* (Shapleigh et al., 1992). Extending these results to the beef heart and *Paracoccus* proteins, we recognize that only one axially bound heme *a* histidine ligand (His-421 in *Rhodobacter* corresponding to His-378 in bovine) originates from a highly conserved region of the polypeptide chain while the second one (*Rhodobacter* His-102, bovine His-61) is located in a region which reveals some remarkable sequence differences for the mammalian and the bacterial protein, i.e., the replacement of Ala-His(61)-Ala-Phe by Tyr-His(102)-Gly-Val. Although it is not known which amino acids constitute the pocket of heme *a*, these simple considerations suggest that the main structural differences may well lie in the amino acid sequence of subunit I. Following this line of argumentation, we would like to note that the histidine ligand of heme a_3 which exhibits much smaller differences between BOX and POX3 originate from a highly conserved region (*Rhodobacter* His-284, bovine His-240).

Such an interpretation implies that the significant structural change of the heme *a* group of the bacterial enzymes upon transition from the fully oxidized to the fully reduced state, i.e., the transformation from the ruffled to the planar geometry, must be associated with a conformational change within subunit I. This is in agreement with the recent study by Haltia (1992), who provided evidence for a redox-linked structural change at the interface between subunits I and II, close to the pockets of heme *a* and heme a_3. It should be noted that the structural changes in heme a_3 occurring upon reduction are qualitatively the same in BOX, POX3, and POX2, giving further support to the idea that the crucial region for the structural control of the active sites in the redox transition is in fact the subunit I/II interface.

ACKNOWLEDGMENT

We gratefully acknowledge the active and generous support of Professor Kurt Schaffner. We also thank Professor Robert Copeland for providing us with preliminary data and helpful comments.

REFERENCES

Aasa, R., Albracht, S. P. J., Falk, K., Lanne, B., & Vannegard, T. (1976) *Biochim. Biophys. Acta 422*, 260–272.

Abe, M., Kitagawa, T., & Kyogoku, Y. (1978) *J. Chem. Phys. 69*, 4526–4534.

Albracht, S. P. J., Van Versefled, H. V., Hagen, W. R., & Kalkman, M. L. (1980) *Biochim. Biophys. Acta 593*, 173–186.

Alden, R. G., Crawford, B. A., Doolen, R., Ondrias, M. R., & Shelnutt, J. A. (1989) *J. Am. Chem. Soc. 111*, 2070–2072.

Anzenbacher, P., Evangelista-Kirkup, R., Schenkman, J., & Spiro, T. G. (1989) *Inorg. Chem. 28*, 4491–4495.

Argade, P. V., Ching, Y.-C., & Rousseau, D. L. (1986) *Biophys. J. 50*, 613–620.

Babcock, G. T. (1988) in *Biological Applications of Resonance Raman Spectroscopy* (Spiro, T. G., Ed.) pp 293–346, Wiley, New York.

Babcock, G. T., & Salmeen, I. (1979) *Biochemistry 18*, 2493–2498.

Babcock, G. T., & Callahan, P. M. (1983) *Biochemistry 22*, 2314–2319.

Babcock, G. T., & Wikström, M. (1992) *Nature 356*, 301–309.

Babcock, G. T., Callahan, P. M., Ondrias, M. R., & Salmeen, I. (1981) *Biochemistry 20*, 959–966.

Berry, E. A., & Trumpower, B. L. (1985) *J. Biol. Chem. 260*, 2458–2467.

Brunori, M., Antonini, G., Malatesta, F., Sarti, P., & Wilson, M. T. (1987) *Adv. Inorg. Biochem. 7*, 93–154.

Buse, G., & Steffens, G. C. M. (1991) *J. Bioenerg. Biomembr. 23*, 269–289.

Centeno, J. A., & Babcock, G. T. (1991) *J. Raman Spectrosc. 22*, 111–117.

Ching, Y.-C., Argade, P. V., & Rousseau, D. L. (1985) *Biochemistry 24*, 4938–4946.

Choi, S., Spiro, T. G., Langry, K. C., & Smith, K. M. (1982) *J. Am. Chem. Soc. 104*, 4337–4344.

Choi, S., Lee, J. J., Wei, Y. H., & Spiro, T. G. (1983) *J. Am. Chem. Soc. 105*, 3692–3707.

Copeland, R. A., & Spiro, T. G. (1986) *FEBS Lett. 197*, 239–243.

Crane, F. L., Glenn, J. L., & Green, D. E. (1956) *Biochim. Biophys. Acta 22*, 475–487.

Czernuszewics, R. S., Li, X.-Y., & Spiro, T. G. (1989) *J. Am. Chem. Soc. 111*, 7024–7031.

Debois, A., & Lutz, M. (1992) *Eur. Biophys. J. 20*, 321–335.

de Paula, J. C., Pfeiffer, W. E., Ingle, R. T., Centeno, J. A., Ferguson-Miller, S., & Babcock, G. T. (1990) *Biochemistry 29*, 8702–8706.

Einarsdóttir, O., Dyer, R. B., Killough, P. M., Fee, J. A., & Woodruff, W. H. (1989) *Proc. SPIE—Int. Soc. Opt. Eng. 1055*, 254–262.

Gregory, L., & Ferguson-Miller, S. (1988) *Ann. N.Y. Acad. Sci. 550*, 260–268.

Haltia, T. (1992) *Biochim. Biophys. Acta 1098*, 343–350.

Haltia, T., Puustinen, A., & Finel, M. (1988) *Eur. J. Biochem. 172*, 543–546.

Han, S., Ching, Y.-C., Hammes, S. L., & Rousseau, D. L. (1991) *Biophys. J. 60*, 45–52.

Hendler, R. W., Pardhasaradhi, K., Reynafarje, B., & Ludwig, B. (1991) *Biophys. J. 60*, 415–423.

Hildebrandt, P. (1990) *Biochim. Biophys. Acta 1040*, 175–186.

Hildebrandt, P., & Stockburger, M. (1989) *Biochemistry 28*, 6722–6728.

Hildebrandt, P., Copeland, R. A., Spiro, T. G., Otlewski, J., Laskowski, M., Jr., & Prendergast, F. G. (1988) *Biochemistry 27*, 5426–5433.

Hildebrandt, P., English, A. M., & Smulevich, G. (1992) *Biochemistry 31*, 2384–2392.

Hosler, J. P., Fetter, J., Tecklenburg, M. M. J., Espe, M., Lerma, C., & Ferguson-Miller, S. (1992) *J. Biol. Chem. 267*, 24264–24272.

Hüther, F.-J., & Kadenbach, B. (1988) *Biochem. Biophys. Res. Commun. 153*, 525–534.

Koyama, Y., Umemoto, Y., Akamatsu, A., Uehara, K., & Tanaka, M. (1986) *J. Mol. Struct. 146*, 273–287.
Li, X.-Y., Czernuszewicz, R. S., Kincaid, J. R., Stein, P., & Spiro, T. G. (1990) *J. Phys. Chem. 94*, 47–61.
Ludwig, B. (1987) *FEMS Microbiol. Rev. 46*, 41–56.
Ludwig, B., & Schatz, G. (1980) *Proc. Natl. Acad. Sci. U.S.A. 77*, 196–200.
Ludwig, B., & Gibson, Q. H. (1981) *J. Biol. Chem. 256*, 10092–10098.
Malmström, B. G. (1990) *Chem. Rev. 90*, 1247–1260.
Parthasarathi, M., Hansen, C., Yamaguchi, S., & Spiro, T. G. (1987) *J. Am. Chem. Soc. 109*, 3865–3871.
Pardhasaradhi, K., Ludwig, B., & Hendler, R. W. (1991) *Biophys. J. 60*, 408–414.
Prendergast, K., & Spiro, T. G. (1992) *J. Am. Chem. Soc. 114*, 3793–3801.
Rousseau, D. L. (1981) *J. Raman Spectrosc. 10*, 94–99.
Saraste, M. (1990) *Q. Rev. Biophys. 23*, 331–366.
Sassaroli, M., Ching, Y.-C., Dasgupta, S., & Rousseau, D. L. (1989) *Biochemistry 28*, 3128–3132.
Schoonover, J. R., Dyer, R. B., Woodruff, W. H., Baker, G. M., Noguchi, M., & Palmer, G. (1988) *Biochemistry 27*, 5433–5440.
Shapleigh, J. P., Hosler, J. P., Tecklenburg, M. M. J., Kim, Y., Babcock, G. T., Gennis, R. B., & Ferguson-Miller, S. (1992) *Proc. Natl. Acad. Sci. U.S.A. 89*, 4786–4790.
Shelnutt, J. A., Medforth, C. J., Berber, M. D., Barkigia, K. M., & Smith, K. M. (1991) *J. Am. Chem. Soc. 113*, 4077–4087.
Sievers, G., Gadsby, P. M. A., Peterson, J., & Thomson, A. J. (1983) *Biochim. Biophys. Acta 742*, 637–647.
Spiro, T. G., & Li, X.-Y. (1988) in *Biological Applications of Resonance Raman Spectroscopy* (Spiro, T. G., Ed.) pp 1–37, Wiley, New York.
Uchida, K., Susai, Y., Hirotani, E., Kimura, T., Yoneya, T., Takeuchi, H., & Harada, I. (1988) *J. Biochem. (Tokyo) 103*, 979–985.
Wikström, M. K. F., Krab, K., & Saraste, M. (1981) *Cytochrome Oxidase. A Synthesis*, Academic Press, London.
Willems, D. L., & Bocian, D. F. (1984) *J. Am. Chem. Soc. 106*, 880–890.